Journal Name

ARTICLE TYPE

Cite this: DOI: 00.0000/xxxxxxxxxx

Supplementary Information: Dynamic correlation suppresses antiferromagnetism in heavily doped Fe-pnictide superconductor $LaFeAsO_{1-x}F_x$

Hrishit Banerjee,*[a,b]

Received Date
Accepted Date

DOI: 00.0000/xxxxxxxxxx

S1 Computational Details

S1.1 DFT Calculations

Our DFT calculations for structural relaxation were carried out in a plane-wave basis with projector-augmented wave (PAW) potentials[1] as implemented in the Vienna Ab-initio Simulation Package (VASP)[2,3].

In all our DFT relaxation calculations, we chose as exchange-correlation functional the GGA implemented following the Perdew-Burke-Ernzerhof (PBESol) prescription[4] for solids. For ionic relaxations using the VASP package, the internal positions of the atoms were allowed to relax until the forces became less than 0.005 eV/Å. An energy cutoff of 600 eV and an 8×8×4 Monkhorst–Pack k-points mesh provided good convergence of the total energy.

The DFT+U calculations were carried out in the form of GGA+U. The value of U at the Fe sites in the GGA+U formalism was 4 eV, in the Liechtenstein Scheme, with J=0.7eV following previous calculations where similar values of U have been selected[5–10].

Hybrid functional calculations were carried out following the prescription of Heyd-Scuseria-Ernzerhof (HSE). The functional used in hybrid calculation can be mathematically expressed as

$$E_{XC}^{HSE}(\sigma) = \alpha E_X^{HF,SR}(\sigma) + (1-\alpha)E_X^{PBE,SR}(\sigma) + E_X^{PBE,LR}(\sigma) + E_C^{PBE}$$

which is the range-separated HSE functional, where α is the fraction of Fock exchange and σ is an adjustable parameter controlling the short-rangeness of the interaction. Here $E_X^{HF,SR}$ denotes the short-range Hartree Fock (HF) exchange functional, $E_X^{PBE,SR}$ denotes the short-range PBE exchange functional, $E_X^{PBE,LR}$ indicates the long-range PBE exchange functional, and E_C^{PBE} refers to the correlation functional as given by PBE. The standard value of $\sigma = 0.2$ along with $\alpha = 0.15$ was used instead of the standard $\alpha = 0.25$ for the tendency of HSE with a high fraction of Fock Exchange to create artificial band gapped states in the case of correlated metals.

The electron localisation function (ELF) is plotted to show bonding, which is defined as a measure of the likelihood of finding an electron in the neighbourhood space of a reference electron located at a given point and with the same spin, and given by the formula[11],

$$ELF = \frac{1}{1+(\frac{D}{D_h})^2}$$

where, $D = \frac{1}{2}\sum_i |\nabla\varphi_i|^2 - \frac{1}{8}\frac{|\nabla\rho|^2}{\rho}$ and $D_h = \frac{3}{10}(3\pi^2)^{5/3}\rho^{5/3}$

Charge density difference calculations have been carried out by the formula

$$\rho_{diff} = \rho_{LaFeAsO_{0.5}F_{0.5}} - \rho_{LaFeAsO}$$

S1.2 DMFT Calculations

For our DFT+DMFT calculations, we are using the full-potential augmented plane-wave basis as implemented in the WIEN2K code package[12]. For the WIEN2K calculations, we used the largest possible muffin-tin radii, and the basis set plane-wave cutoff was defined by $R_{min} \cdot K_{max} = 8.5$, where R_{min} is the muffin-tin radius of the O atoms. The consistency between the VASP and WIEN2K results has always been cross-checked.

DMFT calculations were performed using the TRIQS/DFTTools package[13–15] based on the TRIQS libraries[16]. We perform DMFT calculations in a basis set of projective Wannier functions as implemented in the dmftproj module of TRIQS. It was also used to calculate the initial occupancy of the correlated orbitals. A maximum projection window of −2.5 eV to +3 eV was chosen. All five Fe d orbitals have been treated in the impurity model. The Anderson impurity model, constructed by mapping the many-body

[a] Faculty of Science, Engineering, and Business, University of Dundee, Dundee, Nethergate, Scotland, DD1 4HN, UK, E-mail: hbanerjee001@dundee.ac.uk
[b] School of Metallurgy and Materials Science, University of Birmingham, Edgbaston, Birmingham, B15 2TT, UK.

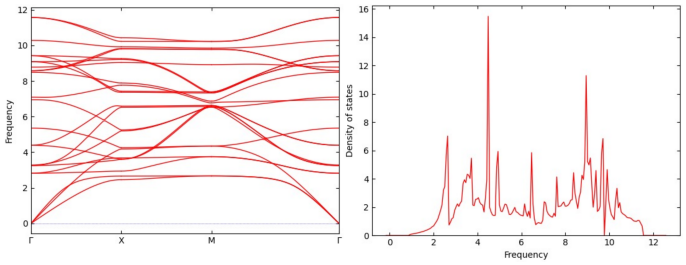

Fig. S1 Phonon bands and phonon DOS showing no negative frequency and hence demonstrating the thermodynamic and dynamic stability of the doped phase of $LaFeAsO_{0.5}F_{0.5}$.

lattice problem to a local problem of an impurity interacting with a bath, was solved using the continuous-time quantum Monte Carlo algorithm in the hybridisation expansion (CT-HYB)[17] as implemented in the TRIQS/CTHYB package[18]. For each DMFT step, 125000×128 cycles of warmup steps and 1250000×128 cycles of measures were performed for the quantum Monte Carlo calculations. We performed one-shot DFT+DMFT calculations, using a fully localised limit (FLL) type double-counting correction[19]. We use a fully rotationally invariant Kanamori Hamiltonian parametrised by Hubbard U and Hund's coupling J_H, where we set the intraorbital interaction to $U' = U - 2J_H$. For our DMFT calculations, we used U = 3.5-4 eV and $J_H = 0.6 - 0.7$ eV following existing literature for Fe d orbitals[5,6,20]. DMFT spectral functions (real-frequency Green's functions) have been obtained using the maximum-entropy method of analytic continuation as implemented in the TRIQS/MAXENT application.[21] The DMFT spectral function may be thought of as a finite temperature correlated Density of State with the impact of electron-electron interaction included, which is missing in DFT. Hence, this may be directly compared to DFT PDOS of Fe. Since DFT lacks electron-electron interactions, it cannot show variation in spectral weights due to self-energy variation hence cannot demonstrate the variation of quasiparticle peak sharpness or quasiparticle weights.

S2 Electronic Structure

In this section, we discuss details of some of the aspects of electronic structure. First, we focus on the dynamical stability of the doped LaFeAsOF system. To this end, we carry out phonon calculations in VASP and examine the phonon band structure and phonon DOS as shown in Fig. S1. We demonstrate that there are no negative frequency modes in either the phonon band structure or the phonon DOS. This proves the dynamical stability of the doped structure conclusively.

Next we investigate the basic differences in electronic structure at the level of GGA+U on doping O in LaFeAsO with 50% F. To this end we calculate the electron localisation function for both the structures and a charge density difference between the structures. These are shown in Fig. S2 (a), and (b). ELF shows the bonding in the structure. There is no significant difference in bonding seen on doping from the ELF. DFT in principle does not capture effect of quasiparticle sharpening which eventually leads to the loss of antiferromagnetic order in the system, because it is a non-interacting one-electron approximation. The charge density

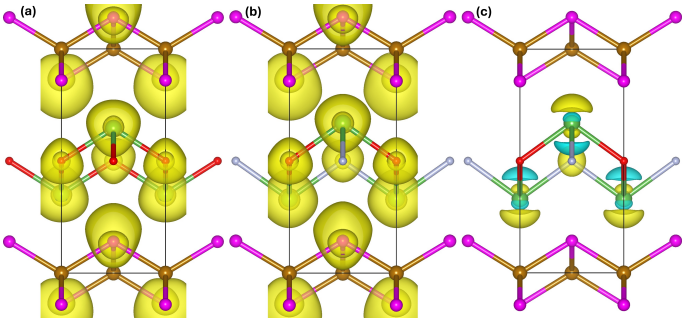

Fig. S2 Figure showing ELF for (a) LaFeAsO, (b) $LaFeAsO_{0.5}F_{0.5}$, and (c) charge density difference plot $\rho_{diff} = \rho_{LaFeAsO_{0.5}F_{0.5}} - \rho_{LaFeAsO}$. In the charge difference plots the yellow isosurfaces show a positive difference i.e. a charge rich region in the doped system while the cyan isosurfaces show a negative difference i.e. a charge depleted region in the dooed system.

Material	LaFeAsO		$LaFeAsO_{0.5}F_{0.5}$	
Magnetic moments				
Site	Fe_1	Fe_2	Fe_1	Fe_2
GGA+U=4eV (μ_B)	2.86	-2.86	2.80	-2.79
GGA+U=3.5eV (μ_B)	2.72	-2.72	2.69	-2.69
HSE (μ_B)	2.49	-2.49	2.45	-2.46
DMFT (μ_B)	2.35	-2.35	0.16	-0.01
Wannier occupancies				
Site	Fe_1	Fe_2	Fe_1	Fe_2
DMFTproj	6.256	6.256	6.317	6.320

Table S1 Table showing magnetic moments for Fe_1 and Fe_2 for LaFeAsO and $LaFeAsO_{0.5}F_{0.5}$ for the GGA+U, HSE, and DMFT calculations.

difference shows a small difference in the charge density around the doped F ion and the ions this F ion is bonded to, however does not show any appreciable difference around the Fe ions, again due to the non-interacting nature of the one-electron DFT.

Magnetic moments and Wannier occupancies are shown in Table S1. Both GGA+U with varying U as well as HSE show antiferromagnetic behaviour for both the pristine and the doped systems, while DMFT shows antiferromagnetic behaviour in the pristine system and suppression of long-range antiferromagnetic order and hence vanishing average moments in the doped system.

Figure S3 shows the DMFT spectral functions in a smaller energy range around the Fermi energy and is resolved according to individual d orbitals to demonstrate the distribution of the dominant orbital characters around the Fermi energy.

Notes and references

1 P. E. Blöchl, *Phys. Rev. B*, 1994, **50**, 17953–17979.
2 G. Kresse and J. Hafner, *Phys. Rev. B*, 1993, **47**, 558–561.
3 G. Kresse and J. Furthmüller, *Phys. Rev. B*, 1996, **54**, 11169–11186.
4 J. P. Perdew, K. Burke and M. Ernzerhof, *Phys. Rev. Lett.*, 1996, **77**, 3865–3868.
5 M. Aichhorn, L. Pourovskii, V. Vildosola, M. Ferrero, O. Parcollet, T. Miyake, A. Georges and S. Biermann, *Phys. Rev. B*, 2009, **80**, 085101.

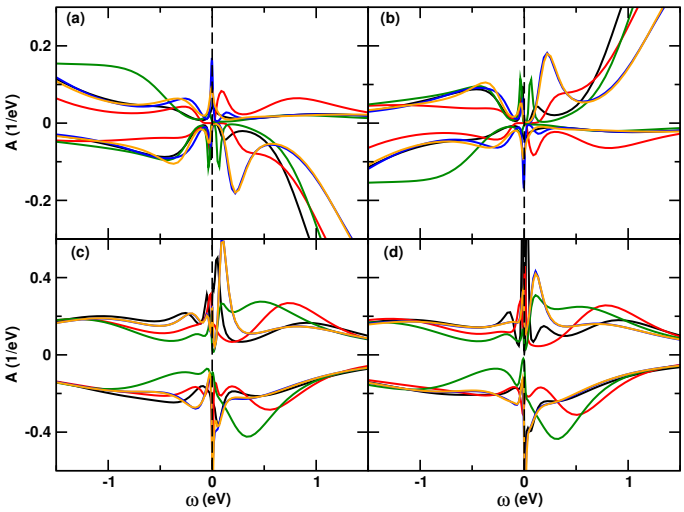

Fig. S3 Figure showing DMFT electronic structure. (a) spectral function for LaFeAsO for Fe_1 site, (b) spectral function for LaFeAsO for Fe_2 site (c) spectral function for $LaFeAsO_{0.5}F_{0.5}$ for Fe_1 site (d) spectral function for $LaFeAsO_{0.5}F_{0.5}$ for Fe_2 site. The different coloured lines indicate the different d orbitals with d_{xy} (black), d_{yz} (red), d_{z^2} (green), d_{xz} (blue) and $d_{x^2-y^2}$ (orange) from dmftproj.

6 M. Aichhorn, L. Pourovskii and A. Georges, *Phys. Rev. B*, 2011, **84**, 054529.

7 H. Banerjee, S. Chakraborty and T. Saha-Dasgupta, *Chemistry of Materials*, 2016, **28**, 8379–8384.

8 H. Banerjee, J. Kaur, M. Nazeeruddin and S. Chakraborty, *Materials Today*, 2022, **60**, 183–200.

9 H. Banerjee, S. Chakraborty and T. Saha-Dasgupta, *Inorganics*, 2017, **5**, 47.

10 H. Banerjee, M. Kumar and T. Saha-Dasgupta, *Phys. Rev. B*, 2014, **90**, 174433.

11 B. Silvi and A. Savin, *Nature*, 1994, **371**, 683–686.

12 P. Blaha, K. Schwarz, F. Tran, R. Laskowski, G. K. H. Madsen and L. D. Marks, *The Journal of Chemical Physics*, 2020, **152**, 074101.

13 M. Aichhorn, L. Pourovskii, V. Vildosola, M. Ferrero, O. Parcollet, T. Miyake, A. Georges and S. Biermann, *Phys. Rev. B*, 2009, **80**, 085101.

14 M. Aichhorn, L. Pourovskii and A. Georges, *Phys. Rev. B*, 2011, **84**, 054529.

15 M. Aichhorn, L. Pourovskii, P. Seth, V. Vildosola, M. Zingl, O. E. Peil, X. Deng, J. Mravlje, G. J. Kraberger, C. Martins, M. Ferrero and O. Parcollet, *Computer Physics Communications*, 2016, **204**, 200 – 208.

16 O. Parcollet, M. Ferrero, T. Ayral, H. Hafermann, I. Krivenko, L. Messio and P. Seth, *Computer Physics Communications*, 2015, **196**, 398 – 415.

17 P. Werner and A. J. Millis, *Phys. Rev. B*, 2006, **74**, 155107.

18 P. Seth, I. Krivenko, M. Ferrero and O. Parcollet, *Computer Physics Communications*, 2016, **200**, 274 – 284.

19 K. Held, *Advances in Physics*, 2007, **56**, 829–926.

20 A. Sarkar, H. Banerjee, D. Das, P. Singh and A. Alam, *Chemistry of Materials*, 2025, **37**, 4607–4616.

21 G. J. Kraberger, R. Triebl, M. Zingl and M. Aichhorn, *Phys. Rev. B*, 2017, **96**, 155128.